Original research article

Journal of Vibration and Control
2026, Vol. 0(0) 1–13

DOI: 10.1177/10775463261450890
journals.sagepub.com/home/jvc
Sage

Prescribed-time sliding mode control for nanopositioning stages via extended state observer

Chunbiao Yang[1], Bo Wang[2], Jin Zhao[1] and Guangwei Wang[1]

Abstract

This paper proposes a synergistic control framework combining a novel prescribed-time extended state observer (PTESO) with a chattering-free prescribed-time sliding mode controller (PTSMC) to achieve high-precision trajectory tracking for piezoelectric nanopositioning stages. The proposed PTESO employs a continuous, bounded time-varying function to accurately estimate lumped disturbances within a user-defined time, thereby obviating the need for complex switching mechanisms. A PTSMC method combining precise disturbance estimation and hyperbolic tangent functions is proposed, which significantly suppresses control chattering while ensuring prescribed-time convergence of the tracking error. Experimental validation demonstrates that our approach achieves superior tracking accuracy and faster user-definable convergence while producing a control signal with improved smoothness, offering a significant advantage over existing advanced control strategies.

Keywords

nanopositioning stage, piezoelectric actuator, prescribed-time control, extended state observer, sliding mode control

Received: 26 November 2025; accepted: 27 April 2026

1. Introduction

Piezoelectric nanopositioning stages have been widely applied in high-precision applications, including biological manipulation, atomic force microscopy, and semiconductor manufacturing, owing to their advantages of fast response, high resolution, and immunity to electromagnetic interference (Lyu and Xu, 2022; Wang et al., 2017; Wang and Xu, 2017; Yang et al., 2020). However, the inherent hysteresis nonlinearity of piezoelectric actuators introduces complex, rate-dependent dynamics between the input voltage and the output displacement, which makes system modeling and parameter identification difficult, thus fundamentally restricting the positioning accuracy and overall performance of the positioning stages (Tao et al., 2022).

To mitigate hysteresis effects, the control strategies in the literature are typically divided into two categories: model-based feedforward control and model-free robust control (Clayton et al., 2009). The former relies on constructing an accurate hysteresis model and compensating for its effects via an inverse model, while the latter treats hysteresis and other uncertainties as a lumped disturbance acting on a nominal linear model. The latter approach simplifies controller design while demanding strong robustness to ensure high performance. Furthermore, nanopositioning stages are often subjected to external disturbances during high-speed operation, which further necessitates a robust control framework capable of actively compensating for disturbance.

Sliding mode control (SMC) is a powerful, robust control technique renowned for its invariance to (matched) disturbances and uncertainties (Lv et al., 2021). However, traditional SMC can only guarantee asymptotic convergence, which has driven the development of finite-time control (Zhao et al., 2020). To enhance convergence speed, researchers have proposed continuous terminal third-order SMC (Xu, 2017) and global fast nonsingular terminal SMC (Wang et al., 2023b), to name a few. Polyakov (2012) further advanced fixed-time stability theory by addressing initial condition dependence. Based on this approach, a fixed-time third-order super-twisting-like SMC for

[1]School of Mechanical Engineering, Guizhou University, Guiyang, China
[2]Department of Mechanical Engineering, The City College of New York, The City University of New York, New York, NY, USA

Corresponding author:
Guangwei Wang, School of Mechanical Engineering, Guizhou University, Guiyang 550025, China.
Email: gwwang@gzu.edu.cn

piezoelectric platforms is designed, which achieves high-precision tracking and rapid convergence (Wang et al., 2021). However, its convergence time bound still implicitly depends on control gains, limiting the ability to preset the convergence time (Guo et al., 2021).

Prescribed-time control has recently emerged as a compelling solution, allowing the system to converge to the equilibrium within a user-specified time (Song et al., 2019, 2023). This framework has been widely applied in prescribed performance control (Song et al., 2025; Song and Sun, 2022), sliding mode control, backstepping control, and other related methods (Chen et al., 2022; Hua et al., 2022). In the field of sliding mode control, Pal et al. (2020) proposed a terminal sliding mode control method with arbitrarily assigned stabilization time, which achieves system stability within a prescribed-time by switching the sliding surface at a specified stabilization moment. For second-order nonlinear systems with matching disturbances, existing research has proposed a prescribed-time nonsingular terminal sliding mode control method by constructing a linear time-varying sliding surface (Shi et al., 2024). However, the time-varying function used in the above schemes tends to infinity at the stabilization moment, which leads to complex controller design and the high-gain problem. Furthermore, the lemma on prescribed-time stability in Shi et al. (2024) is overly stringent, limiting its applicability to certain practical problems. To overcome this limitation, researchers introduced continuously bounded time-varying functions to establish rigorous sufficient conditions for practical prescribed-time stability, thereby providing a more flexible framework (Zeng et al., 2025a, 2025b). Despite these advancements, such flexible frameworks have not yet been fully exploited in SMC strategies.

To suppress the effects of disturbances and uncertainties on the system, Li et al. (2025) proposes a systematic hierarchical disturbance estimation and suppression framework, which utilizes the extended state observer (ESO) to estimate the total disturbance and implement compensation. To compensate for the lumped disturbances in the piezoelectric nanopositioning stage, including hysteresis nonlinearity and external disturbances, a linear ESO was employed for disturbance estimation and was successfully combined with the sliding mode control method (Wang et al., 2023a). Additionally, the integral ESO further enhances estimation performance for unknown nonlinear characteristics by incorporating an integral term into the traditional linear ESO (Chen et al., 2024). Although the aforementioned ESOs achieve asymptotic and finite-time estimation of disturbances, and fixed-time ESOs address time constraints, they still suffer from drawbacks such as conservative convergence and strong dependence on initial conditions and parameters (Sui et al., 2025). For expanding the application of ESO, prior research has introduced a time-varying scaling function to propose PTESO, which can complete disturbance estimation within a prescribed time while suppressing peak phenomena (Cui and Jin, 2021). However, its rapidly growing function characteristics may trigger system oscillations. Based on this, Li et al. (2023) improved the time-varying function and proposed a novel PTESO, but it still suffers from complex control parameters and the risk of inducing chattering. Due to the high accuracy and time requirements of the piezoelectric nanopositioning systems, the precise estimation of hysteresis nonlinearities and external disturbances at a prescribed time is important, and it is crucial to improve the ESO applicable to nanopositioning systems.

To address the above-mentioned challenges, in this paper, we propose a novel practical prescribed-time SMC (PTSMC) strategy integrated with a PTESO for the piezoelectric nanopositioning stage. The main contributions are summarized as follows.

(1) A novel PTESO scheme is presented, which allows flexible specification of state and disturbance estimation times. Compared with the design in Li et al. (2023), the complicated observer switching mechanism is effectively avoided by incorporating continuous time-varying functions.
(2) A PTSMC strategy is proposed by replacing the sign function with a continuous function, which improves the trajectory tracking accuracy and ensures that the system state converges within any preset time. The input chattering issue is substantially reduced relative to the design presented in Shi et al. (2024).
(3) A synergistic control framework integrating PTESO and PTSMC is developed and applied to the nanopositioning system to effectively suppress the influence of lumped disturbances and achieve high-precision motion tracking. Experimental results are presented to illustrate the efficiency and performance of the proposed approach.

The remainder of this paper is organized as follows. Section 2 introduces the dynamical model and preliminary knowledge of the piezoelectric nanopositioning system. Section 3 presents the main results, which include the prescribed-time extended state observer design and the prescribed-time sliding mode control algorithm, along with stability analysis. Section 4 shows the results of both the simulations and experiments. The conclusion of the paper is presented in Section 5.

2. System model and preliminaries

2.1. System model

The dynamics of the piezoelectric nanopositioning stage, depicted in Figure 1, can be represented by the second-order model, following the approach in Xu (2017),

$$m\ddot{x}(t) + b\dot{x}(t) + kx(t) = pu(t) + \Delta(t), \tag{1}$$

where $x(t) \in \mathbb{R}$ is the displacement of the stage; $u(t) \in \mathbb{R}$ is the control input voltage; m, b, k, p represent the

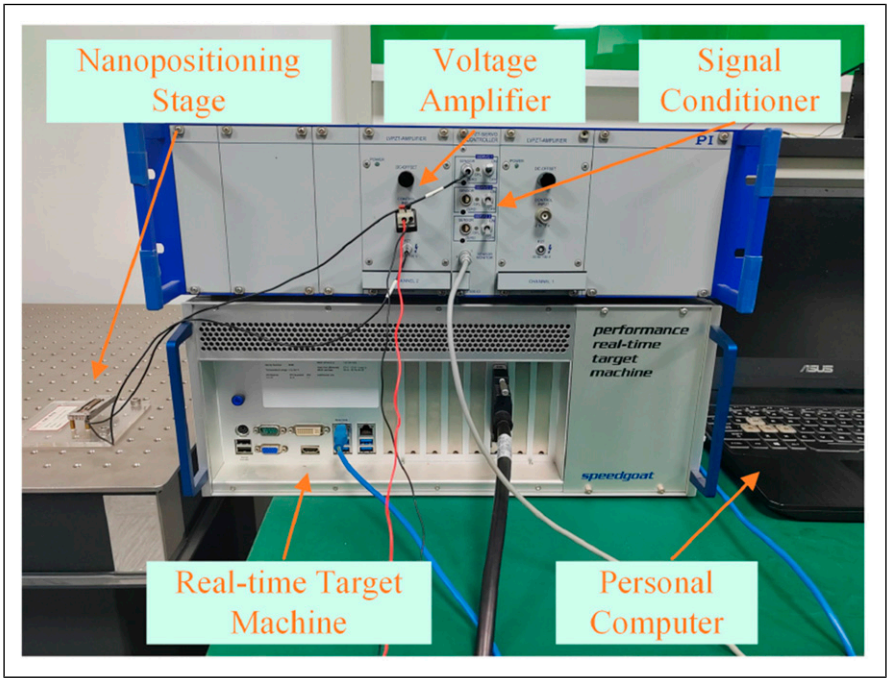

Figure 1. Experimental setup for the piezoelectric nanopositioning stage.

equivalent mass, damping, stiffness, and piezoelectric force coefficients, respectively; and $\Delta(t)$ represents the lumped disturbance, which incorporates the complex hysteresis nonlinearity and any external disturbances.

As illustrated by the experimental results in Figure 2, the hysteresis of the piezoelectric nanopositioning stage exhibits pronounced rate-dependent characteristics, which severely degrade tracking performance and necessitate an advanced control strategy for effective compensation.

To facilitate the controller and observer design, let us define variables $x_1 := x$, $x_2 := \dot{x}$, $d(t) := \Delta(t)/m$. Introducing the intermediate auxiliary state $x_3 := d(t)$, the system model (1) can be rewritten as follows:

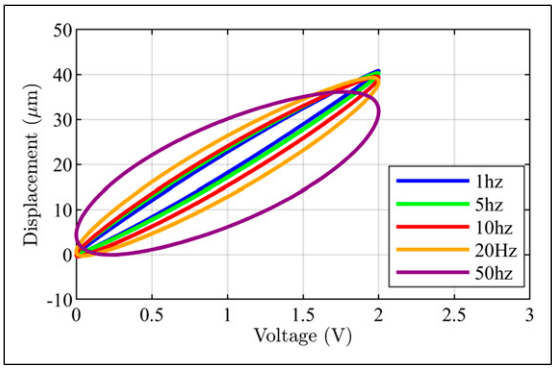

Figure 2. Hysteresis loops of the piezoelectric nanopositioning system.

$$\begin{cases} \dot{x}_1 = x_2 \\ \dot{x}_2 = -a_0 x_1 - a_1 x_2 + b_0 u + x_3, \\ \dot{x}_3 = \dot{d}(t) \end{cases} \tag{2}$$

where $a_0 := k/m$, $a_1 := b/m$, and $b_0 := p/m$.

2.2. Preliminaries on prescribed-time control

Consider the nonlinear system

$$\dot{x} = f(t,x), \quad x(0) = x_0 \tag{3}$$

where $x \in \mathbb{R}^n$ is the system state, $f : \mathbb{R}_{\geq 0} \times \mathbb{R}^n \to \mathbb{R}^n$ is a continuous function. We assume that f is a locally Lipschitz function in x uniformly with respect to t and $f(t, 0) \equiv 0$.

Definition 1. (Zhao et al., 2019). For *the system* (3), if there exist constants $\Omega > 0$ and $T_x > 0$ (in which T_x is defined by the user) such that for any initial condition $x_0 \in \mathbb{R}^n$, it holds that $\|x(t)\| \leq \Omega$ holds for all $t \geq T_x$, then the system (3) is said to have practical prescribed-time stability.

To achieve practical prescribed-time stability, the following continuously bounded time-varying function and its l-th order time derivative $\Gamma^{(l)}$ are defined.

Definition 2. (Zeng et al., 2025b). The function $\Gamma : \mathbb{R}_{\geq 0} \to \mathbb{R}_{\geq 0}$ is defined as

$$\begin{cases} \Gamma(t) := \dfrac{1}{T+\mu-t}, & \Gamma^{(l)}(t) = \dfrac{l!}{(T+\mu-t)^{1+l}}, \quad 0 \leq t < T, \\ \Gamma(t) := \dfrac{1}{\mu}, & \Gamma^{(l)}(t) = 0, \qquad\qquad t \geq T, \end{cases} \tag{4}$$

where T is a positive constant (i.e., the prescribed time) and $\mu \in (0, 1)$ is a regularization time parameter.

It is noted that the function Γ satisfies $\frac{1}{T+\mu} \le \Gamma(t) \le \frac{1}{\mu}$ for all $t \ge 0$, as shown in Figure 3. Moreover, its l-th order time derivative satisfies $0 \le \Gamma^{(l)}(t) < \frac{l!}{\mu^{1+l}}$ for all $t \ge 0$. By appropriately selecting the parameter μ, the designed time-varying function can effectively avoid unbounded gain and singularities.

Lemma 1. (Practical Prescribed-Time Stability). Consider the system (3). If there exist a continuously differentiable, positive definite function $V: \mathbb{R}^n \to \mathbb{R}_{\ge 0}$ and a function $\Gamma(\cdot)$ given in Definition 2 such that

$$\dot{V}(x(t)) \le -\eta \Gamma(t) V(x(t)) + \delta, \tag{5}$$

where $\eta > 0$, $\delta > 0$, then the system (3) is practically prescribed-time stable.

Proof. For $t \in [0, T)$, the following is derived from (5).

(1) If $\eta = 1$, integrating (5) we obtain

$$\begin{aligned} V(x(t)) &\le \left(\frac{T+\mu-t}{T+\mu}\right) V(x(0)) + \delta \int_0^t \frac{T+\mu-t}{T+\mu-\tau} \mathrm{d}\tau, \\ &= \left(\frac{T+\mu-t}{T+\mu}\right) V(x(0)) + \delta (T+\mu-t) \\ &\quad \times \ln\left(\frac{T+\mu}{T+\mu-t}\right). \end{aligned} \tag{6}$$

Then, it follows that

$$\lim_{t \to T} V(x(t)) = \frac{\mu}{T+\mu} V(x(0)) + \delta \mu \ln\left(1 + \frac{T}{\mu}\right). \tag{7}$$

(2) If $\eta \ne 1$, we have that

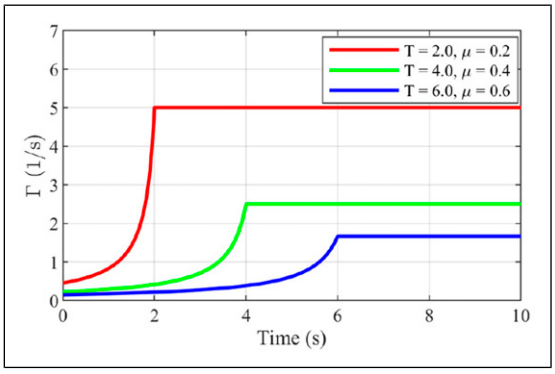

Figure 3. The plot of the time-varying function Γ with different parameters.

$$\begin{aligned} V(x(t)) &\le \left(\frac{T+\mu-t}{T+\mu}\right)^{\eta} V(x(0)) + \delta \int_0^t \frac{(T+\mu-t)^{\eta}}{(T+\mu-\tau)^{\eta}} \mathrm{d}\tau, \\ &= \left(\frac{T+\mu-t}{T+\mu}\right)^{\eta} V(x(0)) + \frac{\delta}{1-\eta} \Big((T+\mu-t)^{\eta} \\ &\quad \times (T+\mu)^{1-\eta} - (T+\mu-t) \Big). \end{aligned} \tag{8}$$

Hence, one gets

$$\begin{aligned} \lim_{t \to T} V(x(t)) &\le \left(\frac{\mu}{T+\mu}\right)^{\eta} V(x(0)) + \frac{\delta}{1-\eta} \Big(\mu^{\eta} \\ &\quad \times (T+\mu)^{1-\eta} - \mu \Big). \end{aligned} \tag{9}$$

For $t \in [T, +\infty)$, it follows from (4) and (5) that

$$V(x(t)) \le \frac{\delta\mu}{\eta} + \left(V(x(T)) - \frac{\delta\mu}{\eta} \right) \exp\left(-\frac{\eta}{\mu} (t - T) \right), \tag{10}$$

which implies that system (3) is practically prescribed-time stable.

Lemma 2. (Jia et al., 2025). For any $\sigma > 0$ and $\chi \in \mathbb{R}$, it holds that

$$0 \le |\chi| - \chi \tanh\left(\frac{\chi}{\sigma}\right) \le 0.2785\sigma. \tag{11}$$

We make the following assumption.

Assumption 1. (Xu, 2017). The lumped disturbance $d(\cdot)$ is assumed to be bounded and differentiable, with its first derivative bounded.

Note that, within the input-output modeling framework and operating regime considered in this work, hysteresis and unmodeled flexible dynamics are reasonably lumped as matched additive disturbances acting on the actuator side, while the input gain is treated as a constant for control analysis and synthesis.

Remark 1. The parameter μ introduces a design margin that regularizes the time-varying gain $\Gamma(t)$ and prevents singular behavior near the prescribed-time boundary. A smaller value of μ leads to convergence of the error system to a smaller residual set within the prescribed time, but typically requires larger controller gains, which may degrade transient behavior. Meanwhile, the settling time T should not be chosen excessively short, as overly aggressive timing can result in large control inputs, increasing the likelihood of actuator saturation and potentially compromising stability and control effectiveness. Therefore, appropriate selection of μ and T, guided by practical constraints, is essential to achieve a desirable balance between steady-state accuracy and transient performance.

3. Main results

The overall prescribed-time control approach proposed in this work is shown in Figure 4, which combines the sliding

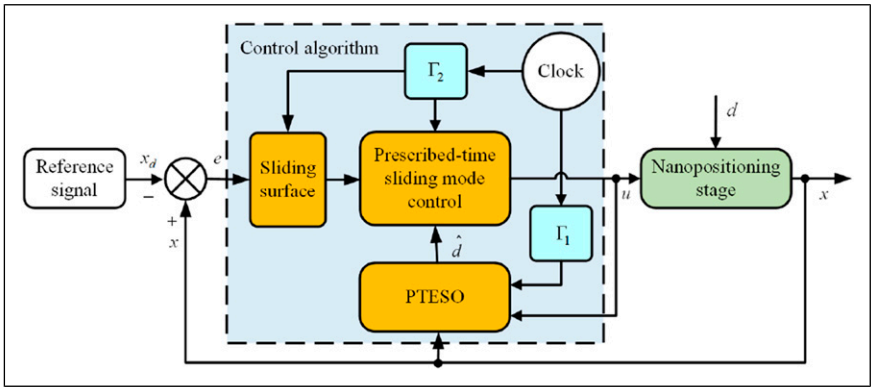

Figure 4. Block diagram of the proposed control framework.

mode control technique, the extended state observer approach, and the practical prescribed-time theory, aiming at realizing the precise control of the piezoelectric nanopositioning stage.

3.1. Prescribed-time extended state observer

Let us use $\widehat{x}_i$ to represent the estimate of x_i, and define the estimation error as $\widetilde{x}_i := x_i - \widehat{x}_i$, for $i \in \{1, 2, 3\}$. The PTESO is designed as

$$\begin{cases} \dot{\widehat{x}}_1 = \widehat{x}_2 + l_1\Gamma_1(t)\rho_0\widetilde{x}_1, \\ \dot{\widehat{x}}_2 = \widehat{x}_3 - a_0x_1 - a_1x_2 + b_0u + l_2\Gamma_1^2(t)\rho_0^2\widetilde{x}_1, \\ \dot{\widehat{x}}_3 = l_3\Gamma_1^3(t)\rho_0^3\widetilde{x}_1, \end{cases} \tag{12}$$

where $\Gamma_1(\cdot)$ is the time-varying function[1] with a prescribed convergence time of T_1 given in Definition 2. The constants l_1, l_2 and l_3 are positive design parameters, and $\rho_0 > 0$ is the correction term.

Subtracting (12) from (2), the estimation error dynamics are given by

$$\begin{cases} \dot{\widetilde{x}}_1 = \widetilde{x}_2 - l_1\Gamma_1(t)\rho_0\widetilde{x}_1, \\ \dot{\widetilde{x}}_2 = \widetilde{x}_3 - l_2\Gamma_1^2(t)\rho_0^2\widetilde{x}_1, \\ \dot{\widetilde{x}}_3 = \dot{d}(t) - l_3\Gamma_1^3(t)\rho_0^3\widetilde{x}_1. \end{cases} \tag{13}$$

In matrix form, (13) can be expressed as

$$\dot{\widetilde{x}} = A\widetilde{x} - \psi(t)LC\widetilde{x} + G(t), \tag{14}$$

where $\widetilde{x} := [\widetilde{x}_1, \widetilde{x}_2, \widetilde{x}_3]^\top$, $\psi(t) := \mathrm{diag}\{\Gamma_1\rho_0, \Gamma_1^2\rho_0^2, \Gamma_1^3\rho_0^3\}$, $L := [l_1, l_2, l_3]^\top$, $C := [1, 0, 0]$, $G(t) := [0, 0, \dot{d}(t)]^\top$, and the matrix

$$A := \begin{bmatrix} 0 & 1 & 0 \\ 0 & 0 & 1 \\ 0 & 0 & 0 \end{bmatrix}.$$

Proposition 1. Consider the system (2) together with the PTESO (12), and let Assumption 1 hold. Then, the estimation error system (13) is practically prescribed-time stable with the prescribed time T_1.

Proof. First, define new state coordinates as $\overline{x} := \overline{\psi}(t)\widetilde{x}$, where $\overline{\psi}(t) := \mathrm{diag}\{\Gamma_1^3\rho_0^3, \Gamma_1^2\rho_0^2, \Gamma_1\rho_0\}$ is invertible. The total derivative of $\overline{x}$ is given by

$$\begin{aligned} \dot{\overline{x}} &= \dot{\overline{\psi}}\widetilde{x} + \overline{\psi}\dot{\widetilde{x}} \\ &= \Gamma_1 Q\overline{\psi}(\overline{\psi}^{-1}\overline{x}) + \overline{\psi}(A(\overline{\psi}^{-1}\overline{x}) - \psi LC(\overline{\psi}^{-1}\overline{x}) + G) \\ &= \Gamma_1 Q\overline{x} + \Gamma_1\rho_0(A - LC)\overline{x} + \overline{\psi}G, \end{aligned} \tag{15}$$

where $Q = \mathrm{diag}\{3, 2, 1\}$.

Considering the Lyapunov candidate $V_{\overline{x}}(\overline{x}) = \overline{x}^\top P\overline{x}$, where $P := [p_{ij}] \in \mathbb{R}^{3\times3}$ is positive definite and symmetric, satisfying $\upsilon_1 I_n \le PQ + Q^\top P \le \upsilon_2 I_n$, where $\upsilon_1, \upsilon_2 > 0$. According to Rayleigh's inequalities, we have

$$\lambda_m(P)\|\overline{x}\|^2 \le V_{\overline{x}}(\overline{x}) \le \lambda_M(P)\|\overline{x}\|^2, \tag{16}$$

where $\lambda_m(\cdot)$ and $\lambda_M(\cdot)$ represent the minimum and maximum eigenvalues of a matrix, respectively. In addition, there exists $\gamma > 0$ such that the following inequality holds

$$(A - LC)^\top P + P(A - LC) \le A + A^\top - \gamma I_n. \tag{17}$$

Taking time derivative of $V_{\overline{x}}$, one gets

$$\begin{aligned} \dot{V}_{\overline{x}}(\overline{x}) &= \dot{\overline{x}}^\top P\overline{x} + \overline{x}^\top P\dot{\overline{x}}, \\ &= \Gamma_1\overline{x}^\top\left(Q^\top P + PQ\right)\overline{x} + \Gamma_1\rho_0\overline{x}^\top\left((A - LC)^\top P \right. \\ &\quad \left. + P(A - LC)\right)\overline{x} + G^\top\overline{\psi}^\top P\overline{x} + \overline{x}^\top P\overline{\psi}G \\ &\le \Gamma_1\overline{x}^\top(QP + PQ)\overline{x} + \Gamma_1\rho_0\overline{x}^\top\left(A^\top + A - \gamma I_n\right)\overline{x} \\ &\quad + G^\top\overline{\psi}^\top P\overline{x} + \overline{x}^\top P\overline{\psi}G \\ &\le \upsilon_2\Gamma_1\|\overline{x}\|^2 + 2\Gamma_1\rho_0\|A\|\|\overline{x}\|^2 - \Gamma_1\rho_0\gamma\|\overline{x}\|^2 \\ &\quad + 6\overline{P}\Gamma_1\rho_0\|\dot{d}\|\|\overline{x}\|, \end{aligned} \tag{18}$$

where $\overline{P} = \max\{|p_{13}|, |p_{23}|, |p_{31}|, |p_{32}|, |p_{33}|\}$. It follows from Young's inequality that

$$6\overline{P}\Gamma_1\rho_0\|\dot{d}\|\|\bar{x}\| \le \varepsilon\Gamma_1\rho_0\|\bar{x}\|^2 + \frac{\Gamma_1\rho_0}{\varepsilon}\left(3\overline{P}\|\dot{d}\|\right)^2, \tag{19}$$

where $\varepsilon > 0$. By choosing $\rho_0 \ge \upsilon_2$, $\gamma \ge (1 + 2\|A\| + \varepsilon)$, and utilizing (16), one obtains

$$\begin{aligned}\dot{V}_{\bar{x}}(\bar{x}) &\le \upsilon_2\Gamma_1\|\bar{x}\|^2 + 2\Gamma_1\rho_0\|A\|\|\bar{x}\|^2 - \Gamma_1\rho_0(\gamma-\varepsilon)\|\bar{x}\|^2 \\ &\quad + \frac{\Gamma_1\rho_0}{\varepsilon}\left(3\overline{P}\|\dot{d}\|\right)^2 \\ &\le \rho_0\Gamma_1\|\bar{x}\|^2 + 2\Gamma_1\rho_0\|A\|\|\bar{x}\|^2 - \Gamma_1\rho_0(\gamma-\varepsilon)\|\bar{x}\|^2 \\ &\quad + \frac{\Gamma_1\rho_0}{\varepsilon}\left(3\overline{P}\|\dot{d}\|\right)^2 \\ &\le -\frac{\rho_0(\gamma-\varepsilon-2\|A\|-1)}{\lambda_M(P)}\Gamma_1\|\bar{x}\|^2 + \frac{\Gamma_1\rho_0}{\varepsilon}\left(3\overline{P}\|\dot{d}\|\right)^2 \\ &= -\eta_{\bar{x}}\Gamma_1 V_{\bar{x}}(\bar{x}) + \frac{\Gamma_1\rho_0}{\varepsilon}\left(3\overline{P}\|\dot{d}\|\right)^2,\end{aligned} \tag{20}$$

where $\eta_{\bar{x}} = \rho_0(\gamma - \varepsilon - 2\|A\| - 1)/\lambda_M(P) > 0$, and $\|\dot{d}\| \le d_0$ with $d_0 > 0$. Note that $\Gamma_1(t) \le 1/\mu_1$ for all $t \ge 0$, we then obtain

$$\dot{V}_{\bar{x}}(\bar{x}) \le -\eta_{\bar{x}}\Gamma_1 V_{\bar{x}}(\bar{x}) + \delta_{\bar{x}}, \tag{21}$$

where

$$\delta_{\bar{x}} := \frac{\rho_0}{\varepsilon\mu_1}\left(3\overline{P}d_0\right)^2$$

is a positive constant.

According to Lemma 1, for all $t \ge T_1$,

$$V_{\bar{x}}(t) \le \frac{\delta_{\bar{x}}\mu_1}{\eta_{\bar{x}}} + \left(V_{\bar{x}}(T_1) - \frac{\delta_{\bar{x}}\mu_1}{\eta_{\bar{x}}}\right)\exp\left(-\frac{\eta_{\bar{x}}}{\mu_1}(t - T_1)\right). \tag{22}$$

Hence, $V_{\bar{x}}(t)$ is bounded for $t \ge T_1$. In particular, define

$$V_{\bar{x},\max} := \max\left\{V_{\bar{x}}(T_1),\ \frac{\delta_{\bar{x}}\mu_1}{\eta_{\bar{x}}}\right\}.$$

Then $V_{\bar{x}}(t) \le V_{\bar{x},\max}$ for all $t \ge T_1$. Using (16), we obtain the following constant bound:

$$\|\bar{x}(t)\| \le \overline{X} := \sqrt{\frac{V_{\bar{x},\max}}{\lambda_m(P)}}, \quad \forall t \ge T_1.$$

Therefore,

$$\|\widetilde{x}(t)\| = \|\overline{\psi}^{-1}(t)\bar{x}(t)\| \le \|\overline{\psi}^{-1}(t)\|\overline{X}, \quad \forall t \ge T_1. \tag{23}$$

Since $\Gamma_1(t) = 1/\mu_1$ for $t \ge T_1$, $\overline{\psi}^{-1}(t)$ is bounded for $t \ge T_1$. Let $\kappa_\psi := \sup_{t\ge T_1}\|\overline{\psi}^{-1}(t)\|$, then

$$\|\widetilde{x}(t)\| \le \widetilde{X} := \kappa_\psi\overline{X}, \quad \forall t \ge T_1,$$

which completes the proof.

3.2. PTSMC design based on PTESO

In this section, a composite control strategy incorporating PTESO and PTSMC is proposed. The PTESO provides real-time disturbance compensation, while the PTSMC guarantees prescribed-time convergence of the tracking error and robustness against residual estimation errors.

First, the displacement and velocity tracking errors are denoted by

$$e_1 := x_1 - x_d(t), \quad e_2 := x_2 - \dot{x}_d(t), \tag{24}$$

where $x_d(t)$ is the desired trajectory. Define two auxiliary variables as $z_1 := \Gamma_2(t)e_1$ and $z_2 = \dot{z}_1$. Then, let us design the prescribed-time sliding surface as

$$s(t,z) := z_2 + c_1 z_1 + c_2\Gamma_2(t)z_1, \tag{25}$$

where $c_1 > 0$, $c_2 > 0$, $z := [z_1, z_2]^\top$, and $\Gamma_2(\cdot)$ is the scaling function with a prescribed stabilization time T_2. To ensure that the disturbance is effectively estimated before the controller fully converges, let us set $T_1 < T_2$.

The prescribed-time control law is designed as

$$\begin{aligned}u = \frac{1}{b_0}\Big(&a_0x_1 + a_1x_2 - \widehat{d} + \ddot{x}_d - \ddot{\Gamma}_2\Gamma_2^{-1}e_1 - 2\dot{\Gamma}_2\Gamma_2^{-1}e_2 \\ &-c_1\Gamma_2^{-1}z_2 - c_2\dot{\Gamma}_2\Gamma_2^{-1}z_1 - c_2z_2 - k_1s - k_2\tanh\left(\frac{s}{k_0}\right)\Big),\end{aligned} \tag{26}$$

where $\widehat{d} = \widehat{x}_3$ is the estimated value of the lumped disturbance. The parameters satisfy the conditions: $k_0 > 0$ and $k_2 > |\widetilde{d}|$, where $\widetilde{d} = d - \widehat{d}$, which represents the disturbance observation error in PTESO. To avoid the chattering induced by the discontinuous function sign(s), we introduce the hyperbolic tangent function $\tanh(s/k_0)$.

Proposition 2. For the system (2), the proposed control law (26) integrated with the PTESO (12), guarantees that the closed-loop system is practically prescribed-time stable, and the tracking errors e_1 and e_2 converge within the prescribed time T_2.

Proof. Differentiating the sliding mode variable (25) and substituting into (2) yields

$$\begin{aligned}\dot{s} &= \dot{z}_2 + c_1\dot{z}_1 + c_2\dot{\Gamma}_2z_1 + c_2\Gamma_2\dot{z}_1 \\ &= \ddot{\Gamma}_2e_1 + 2\dot{\Gamma}_2e_2 + \Gamma_2(-a_0x_1 - a_1x_2 + b_0u + d - \ddot{x}_d) \\ &\quad + c_1z_2 + c_2\dot{\Gamma}_2z_1 + c_2\Gamma_2z_2.\end{aligned} \tag{27}$$

Substituting the control law (26) into (27) results in the closed-loop sliding mode dynamics:

$$\dot{s} = \Gamma_2\left(\widetilde{d} - k_1s - k_2\tanh\left(\frac{s}{k_0}\right)\right). \tag{28}$$

Consider the Lyapunov function candidate $V_s = 1/2s^2$. Taking time derivative of V_s and according to Lemma 2 yields

$$\begin{aligned}\dot{V}_s &= s\dot{s}=\Gamma_2\left(\widetilde{d}s-k_1s^2-k_2s\tanh\left(\frac{s}{k_0}\right)\right)\\ &\le -k_1\Gamma_2s^2-k_2\Gamma_2s\tanh\left(\frac{s}{k_0}\right)+\Gamma_2|s||\widetilde{d}|\\ &= -k_1\Gamma_2s^2-k_2\Gamma_2s\tanh\left(\frac{s}{k_0}\right)+k_2\Gamma_2|s|-k_2\Gamma_2|s|+\Gamma_2|s||\widetilde{d}|\\ &\le -k_1\Gamma_2s^2+k_2\Gamma_2\left(|s|-s\tanh\left(\frac{s}{k_0}\right)\right)\\ &\le -\eta_s\Gamma_2V_s+\delta_s,\end{aligned} \tag{29}$$

where $\eta_s = 2k_1$ and $\delta_s = 0.2785k_0k_2/\mu_2$.

Based on Lemma 1, for $t \ge T_2$ we have

$$V_s(t)\le\frac{\delta_s\mu_2}{\eta_s}+\left(V_s(T_2)-\frac{\delta_s\mu_2}{\eta_s}\right)\exp\left(-\frac{\eta_s}{\mu_2}(t-T_2)\right). \tag{30}$$

Hence, $V_s(t) \le V_{s,\max}$ for all $t \ge T_2$, where

$$V_{s,\max} := \max\left\{V_s(T_2),\ \frac{\delta_s\mu_2}{\eta_s}\right\}.$$

Therefore, there exists a constant $S > 0$ such that

$$\|s(t)\| \le S := \sqrt{2V_{s,\max}}, \quad \forall t \ge T_2. \tag{31}$$

Then, we have

$$\dot{z}_1 = -c_1z_1 - c_2\Gamma_2z_1 + s. \tag{32}$$

Choosing the Lyapunov function candidate $V_{z_1} = \frac{1}{2}z_1^2$ and differentiating it along (32) yields

$$\begin{aligned}\dot{V}_{z_1} &= z_1\dot{z}_1 = -c_1z_1^2 - c_2\Gamma_2z_1^2 + z_1s\\ &\le -c_1z_1^2 - c_2\Gamma_2z_1^2 + |z_1|\|s\| \le -c_1z_1^2 - c_2\Gamma_2z_1^2 + |z_1|\overline{S}\\ &\le -c_1z_1^2 - c_2\Gamma_2z_1^2 + \frac{\varepsilon_z}{2}z_1^2 + \frac{1}{2\varepsilon_z}\overline{S}^2\\ &\le -\eta_{z_1}\Gamma_2V_{z_1} + \delta_{z_1},\end{aligned} \tag{33}$$

where $\eta_{z_1} = 2c_2$, $0 < \varepsilon_z < 2c_1$, and $\delta_{z_1} = \overline{S}^2/2\varepsilon_z$. According to Lemma 1, s is bounded throughout both the reaching and steady-state phases. This ensures the existence of an upper bound $\overline{S} > 0$ ($\|s\| \le \overline{S}$), where $\overline{S} = S$ for $t \ge T_2$. Consequently, $V_{z_1}(t)$ is bounded for all $t \ge T_2$. In particular, for all $t \ge T_2$, we have that

$$V_{z_1}(t) \le V_{z_1,\max} := \max\left\{V_{z_1}(T_2),\ \frac{\delta_{z_1}\mu_2}{\eta_{z_1}}\right\},$$

and thus there exists a constant $Z_I > 0$ such that

$$\|z_1(t)\| \le Z_I := \sqrt{2V_{z_1,\max}}, \quad \forall t \ge T_2. \tag{34}$$

Then, from $z_1 = \Gamma_2e_1$ and the fact that $\Gamma_2(t) = \frac{1}{\mu_2}$ for $t \ge T_2$, it follows that

$$\begin{aligned}\|e_1(t)\| &= \Gamma_2^{-1}\|z_1(t)\| = \mu_2\|z_1(t)\|\\ &\le E_I := \mu_2Z_I, \quad \forall t \ge T_2.\end{aligned} \tag{35}$$

That is, e_1 enters the residual set $\{\|e_1\| \le E_I\}$ at $t = T_2$ and remains bounded thereafter.

Next, from $z_2 = \dot{z}_1$ and $z_2 = \dot{\Gamma}_2e_1 + \Gamma_2e_2$, we have

$$\Gamma_2e_2 = z_2 - \dot{\Gamma}_2e_1.$$

Moreover, $z_2 = s - c_1z_1 - c_2\Gamma_2z_1$. Therefore,

$$\begin{aligned}\Gamma_2\|e_2\| &= \|z_2 - \dot{\Gamma}_2e_1\| \le \|z_2\| + |\dot{\Gamma}_2|\|e_1\|\\ &\le \|s\| + c_1\|z_1\| + c_2\Gamma_2\|z_1\| + |\dot{\Gamma}_2|\|e_1\|\\ &\le S + c_1Z_I + c_2\Gamma_2Z_I + |\dot{\Gamma}_2|E_I, \quad \forall t \ge T_2.\end{aligned} \tag{36}$$

Noting that $\dot{\Gamma}_2(t) = 0$ for $t \ge T_2$, it follows from (36) that

$$\begin{aligned}\|e_2(t)\| &\le E_{II} := \Gamma_2^{-1}S + (c_1\Gamma_2^{-1} + c_2)Z_I\\ &= \mu_2S + (c_1\mu_2 + c_2)Z_I, \quad \forall t \ge T_2.\end{aligned} \tag{37}$$

Finally, $\|e_1(t)\| \le E_I$ and $\|e_2(t)\| \le E_{II}$ for all $t \ge T_2$, indicating that the tracking error system is practically prescribed-time stable.

Remark 2. As stated in Definition 1, the settling time is required to be user-prescribed and independent of the initial conditions, meaning that it can be arbitrarily specified. However, the convergence is to a residual set. We acknowledge that the radius of this residual set implicitly depends on the system gains, design parameters, and the disturbance bound, but it is tunable based on design requirements, as established in the proofs of Lemma 1 and Propositions 1 and 2.

Remark 3. All control gains and design parameters (e.g., μ, ε_z, Γ) carry appropriate physical units to ensure that the derived control laws and residual bounds are dimensionally consistent with the system states.

Remark 4. Note that within the closed-loop system, the practical prescribed-time convergence of the estimation error subsystem together with the forward completeness and zero-input global asymptotic stability of the tracking error subsystem prevents the peaking-induced instability mechanisms typically encountered in general nonlinear systems.

4. Simulation and experimental results

In this section, the performance of the proposed PTESO-based PTSMC strategy is shown through both simulations and experiments on the piezoelectric nanopositioning stage.

4.1. Simulation results

The simulations were conducted using the identified model parameters of the nanopositioning stage from Wang et al. (2023a). That is, $a_0 = 3.2066 \times 10^6$, $a_1 = 2372$, $b_0 = 5.255 \times 10^7$. All parameters are in SI units. To emulate the complex

and time-varying nature of hysteresis and external disturbances, a lumped disturbance was introduced, defined as $d(t) := 5 \times 10^5 \sin(20\pi(t+2))$. The desired trajectory was set to a sinusoidal signal, that is, $x_d(t) := 10 \sin(20\pi t - \pi/2) + 10$. To evaluate the independence from initial conditions, simulations were initiated from two distinct states: $x(0) = [5,0]^\top$ and $x(0) = [20,0]^\top$. In addition, to illustrate the convergence effect of the observers, the initial disturbance estimate is defined as $\hat{d}(0) = 1 \times 10^6$.

To validate the superiority of the proposed method, the proposed PTESO-based PTSMC is compared with the prescribed-time nonsingular sliding mode control (PTNSMC) (Shi et al., 2024) based on switching PTESO (Li et al., 2023) (SPTESO-based PTNSMC). The governing equations for the SPTESO are given by

$$\begin{aligned}
\dot{\hat{x}}_1 &= \hat{x}_2 + \Lambda\theta\varphi_1\tilde{x}_1 + (1-\Lambda)\cdot\xi_1\lceil\tilde{x}_1\rfloor^{\alpha_1},\\
\dot{\hat{x}}_2 &= \hat{x}_3 - a_0x_1 - a_1x_2 + b_0u + \Lambda\theta^2\varphi_2\tilde{x}_1 + (1-\Lambda)\cdot\xi_2\lceil\tilde{x}_1\rfloor^{\alpha_2},\\
\dot{\hat{x}}_3 &= \Lambda\theta^3\varphi_3\tilde{x}_1 + (1-\Lambda)\cdot\xi_3\lceil\tilde{x}_1\rfloor^{\alpha_3},
\end{aligned} \tag{38}$$

where $\lceil\cdot\rfloor^{\alpha} := |\cdot|^{\alpha}\mathrm{sign}(\cdot)$, $\varphi_1 = 2.75 \times 10^3$, $\varphi_2 = 3.025 \times 10^6$, $\varphi_3 = 6.24 \times 10^8$ and $\xi_1 = 1.524 \times 10^4$, $\xi_2 = 1.1 \times 10^8$, $\xi_3 = 9.5 \times 10^{10}$ are the correction terms. The constants are given by $\alpha_1 = 2/3$, $\alpha_2 = 1/3$ and $\alpha_3 = 0$. The time-switching function Λ and the time-varying function θ are defined as:

$$\begin{aligned}
\Lambda(t) &:= \begin{cases} 1, & t \in [0, T_1), \\ 0, & t \in [T_1, +\infty), \end{cases}\\
\theta(t) &:= \begin{cases} \dfrac{T_1}{T_1 - t}, & t \in [0, T_1), \\ 1, & t \in [T_1, +\infty), \end{cases}
\end{aligned} \tag{39}$$

with $T_1 = 0.01$. The SPTESO-based PTNSMC is designed as

$$\begin{aligned}
u = \frac{1}{b_0}\Big(&-c_P\dot{\Theta}(x_1 - x_d) - c_P\Theta(x_2 - \dot{x}_d) - k_3\Theta s\\
&+ \ddot{x}_d + a_0x_1 + a_1x_2 - \hat{d} - k_4\mathrm{sign}(s_P)\Big),
\end{aligned} \tag{40}$$

where $s_P = x_2 - \dot{x}_d + c_P\theta(x_1 - x_d)$, $c_P = 20$, $k_3 = 20$, $k_4 = 1 \times 10^6$. The time-varying function is

$$\Theta(t) := \begin{cases} \dfrac{T_2}{T_2 - t}, & t \in [0, T_2), \\ 1, & t \in [T_2, +\infty). \end{cases} \tag{41}$$

The controller convergence time is $T_2 = 0.1$.

For a fair comparison, the parameters for the PTSMC are set to $c_1 = 10$, $c_2 = 10$, $k_0 = 3 \times 10^3$, $k_1 = 20$, $k_2 = 1 \times 10^6$, and $\mu_2 = 0.01$. The parameters of the proposed PTESO are $l_1 = 10$, $l_2 = 40$, $l_3 = 30$, $\rho_0 = 55$ and $\mu_1 = 0.02$. Moreover, two different sets of convergence times are chosen: $[T_1, T_2] = [0.01, 0.1]$ and $[T_1, T_2] = [0.03, 0.05]$.

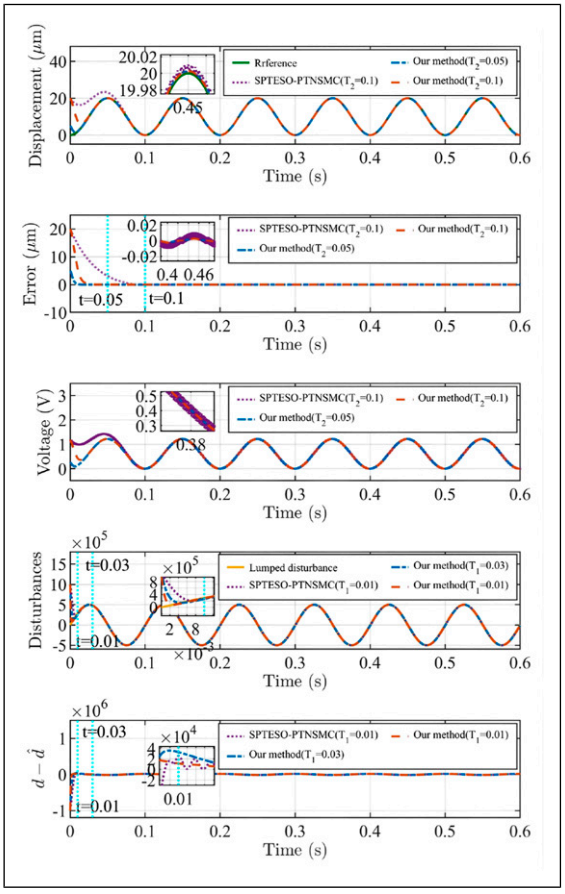

Figure 5. Comparison of simulation results for sinusoidal trajectory tracking.

The simulation results of trajectory tracking and error estimation are shown in Figure 5, demonstrating that the proposed controller successfully forces the tracking error to converge within the prescribed times of 0.05 and 0.1, respectively, regardless of the initial conditions. This validates the prescribed-time convergence capability of the proposed PTSMC. Furthermore, error comparison demonstrates that the proposed control strategy exhibits higher tracking accuracy compared to the SPTESO-based PTNSMC. The control input (Voltage) profiles show that the proposed method effectively avoids chattering in the control input by employing the hyperbolic tangent function. The lumped disturbance and estimation error profiles demonstrate the superiority of the proposed PTESO, which achieves disturbance observation within the preset time while avoiding the chattering caused by SPTESO. The maximum disturbance estimation errors for the two methods are 1.62×10^4 and 1.33×10^4, respectively, with PTESO achieving 17.9% higher accuracy than SPTESO. This improvement enhances the precision of disturbance compensation, thereby improving the system tracking performance.

4.2. Experimental results

The experimental validation was performed on the piezoelectric nanopositioning platform shown in Figure 1. The setup consists of a flexible-hinge stage (Model: PI P-603.3S2), which features an integrated piezoelectric actuator and a strain gauge sensor. The stage has a maximum travel range of 380 μm and operates with excitation voltages from −20 V to +120 V. The Speedgoat real-time target machine serves as the control core, executing the control algorithm online. Real-time commands are sent from a host computer to the target machine, which interfaces with the platform via a Speedgoat IO133 data acquisition board. The control voltage computed by the algorithm was amplified tenfold by a voltage amplifier (PI E-505.00S) before being applied to the piezoelectric actuator. The sampling frequency was set to 10 kHz.

To comprehensively evaluate the performance of the proposed control strategy, the proposed method is compared with the conventional sliding mode control based on the finite-time extended state observer (Sun et al., 2015) (FTESO-based CSMC) and SPTESO-based PTNSMC.

The finite-time extended state observer (Sun et al., 2015) is given by

$$\begin{cases} \dot{\widehat{x}}_1 = \widehat{x}_2 + \overline{\eta}_1 \widetilde{x}_1, \\ \dot{\widehat{x}}_2 = \widehat{x}_3 - a_0 x_1 - a_1 x_2 + b_0 u + \overline{\eta}_2 \lceil \widetilde{x}_1 \rfloor^{\overline{\alpha}_1}, \\ \dot{\widehat{x}}_3 = \overline{\eta}_3 \lceil \widetilde{x}_1 \rfloor^{\overline{\alpha}_2}, \end{cases} \tag{42}$$

where the parameters satisfy $\overline{\eta}_1 > 0, \overline{\eta}_2 > 0, \overline{\eta}_3 > 0, 0 < \overline{\alpha}_1 < 1$, $0 < \overline{\alpha}_2 < 1$. Then, the FTESO-based CSMC is as follows:

$$u = \frac{1}{b_0}\Big(-c_C(x_2 - \dot{x}_d) + \ddot{x}_d + a_0 x_1 + a_1 x_2 - \widehat{d} - k_5 s - k_6 \mathrm{sign}(s_C)\Big). \tag{43}$$

where $s_C = x_2 - \dot{x}_d + c_C(x_1 - x_d)$, $c_C > 0, k_5 > 0$ and $k_6 > 0$.

The control parameters for the method proposed in this paper and the other two control methods are shown in Table 1. Since the parameter scales vary significantly across different observer/controller architectures, we adopted *matched settling time* as the primary tuning criterion to ensure a fair and meaningful evaluation. Specifically, the parameters of all comparative methods were tuned such that their closed-loop systems exhibit similar convergence rates (settling times) under the nominal step response.

Table 1. Parameters of the controllers.

Control scheme	Parameter values
Our method	l_1 = 16, l_2 = 20, l_3 = 25, ρ_0 = 20, μ_1 = 0.02, T_1 = 0.02, T_2 = 0.04, μ_2 = 0.01, c_1 = 10, c_2 = 20, k_0 = 300, k_1 = 20, k_2 = 1 × 10^6
SPTESO-based PTNSMC	φ_1 = 960, φ_2 = 7.2 × 10^4, φ_3 = 5.4 × 10^6, ξ_1 = 2878, ξ_2 = 3.94 × 10^6, ξ_3 = 6.4 × 10^8, α_1 = 2/3, α_2 = 1/3, α_3 = 0, T_1 = 0.02 T_2 = 0.04, c_P = 20, k_3 = 20, k_4 = 2 × 10^6
FTESO-based CSMC	$\overline{\eta}_1$ = 400, $\overline{\eta}_2$ = 1 × 10^4, $\overline{\eta}_3$ = 5 × 10^8, $\overline{\alpha}_1$ = 0.6, $\overline{\alpha}_2$ = 0.4, c_C = 200, k_5 = 100, k_6 = 2 × 10^6

Figure 6 presents the comparative experimental results of control performance for a 5 Hz sine trajectory. From the displacement trajectories and the corresponding tracking error profiles, it is observed that although the convergence time of the FTESO-based CSMC method attempts to approach the prescribed termination instant, it still exhibits significant chattering phenomena during the steady-state phase. In contrast, the proposed method achieves a smoother transient response without noticeable overshoot while realizing prescribed-time convergence. Combined with the quantitative data in Table 2, the proposed method significantly reduces the maximum position tracking error (MPTE) by 54.1% and 70.3% compared to the FTESO-based CSMC and SPTESO-based PTNSMC, respectively.

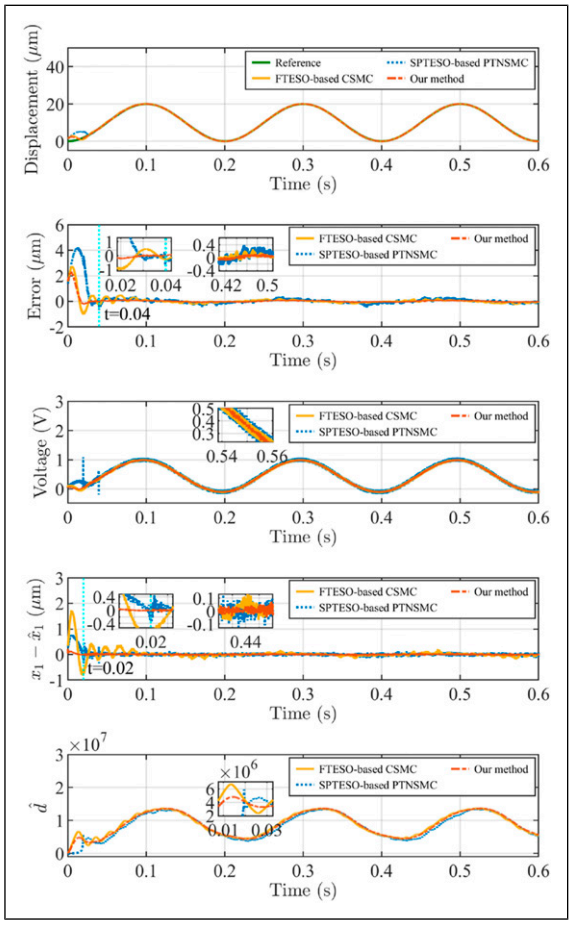

Figure 6. Comparative analysis of experimental results for 5-Hz sine wave trajectory tracking.

Table 2. Performance indicators of different control schemes.

Signal	Error	FTESO-based CSMC	SPTESO-based PTNSMC	Our method
5 Hz Sine wave	MPTE	0.266	0.412	0.122
	IAE	0.114	0.151	0.052
	ITAE	0.019	0.023	0.009
20 Hz Sine wave	MPTE	2.547	3.438	0.694
	IAE	0.749	1.021	0.298
	ITAE	0.174	0.249	0.047
Composite signal	MPTE	0.891	1.348	0.443
	IAE	0.193	0.266	0.129
	ITAE	0.099	0.132	0.061

Furthermore, the state estimation error profiles $(x_1 - \widehat{x}_1)$ and the estimated disturbance profiles $(\widehat{d})$ highlight the performance differences among the three extended state observers. The results indicate that the maximum estimation errors of the FTESO and SPTESO are 0.22 and 0.15, respectively, whereas the maximum error of the proposed PTESO is only 0.08. Meanwhile, while the SPTESO ensures state estimation within the prescribed time, it exhibits distinct oscillations in position and disturbance estimates at the switching time of 0.02 due to the discontinuous switching function. These results forcefully demonstrate that the observer and sliding mode controller architecture based on continuous time-varying functions not only ensures convergence within the prescribed time but also significantly enhances the state estimation precision and trajectory tracking accuracy of the nanopositioning system.

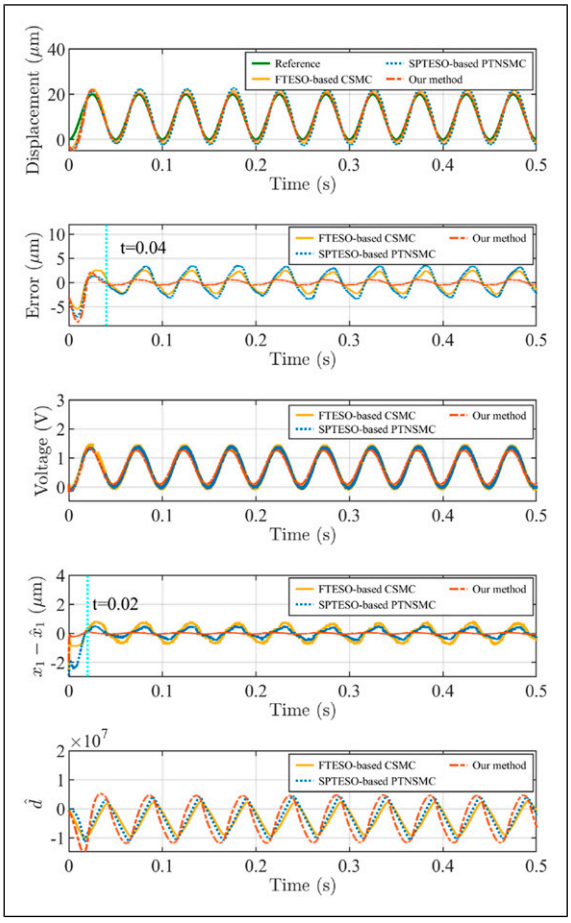

Figure 7. Comparative analysis of experimental results for 20-Hz sine wave trajectory tracking.

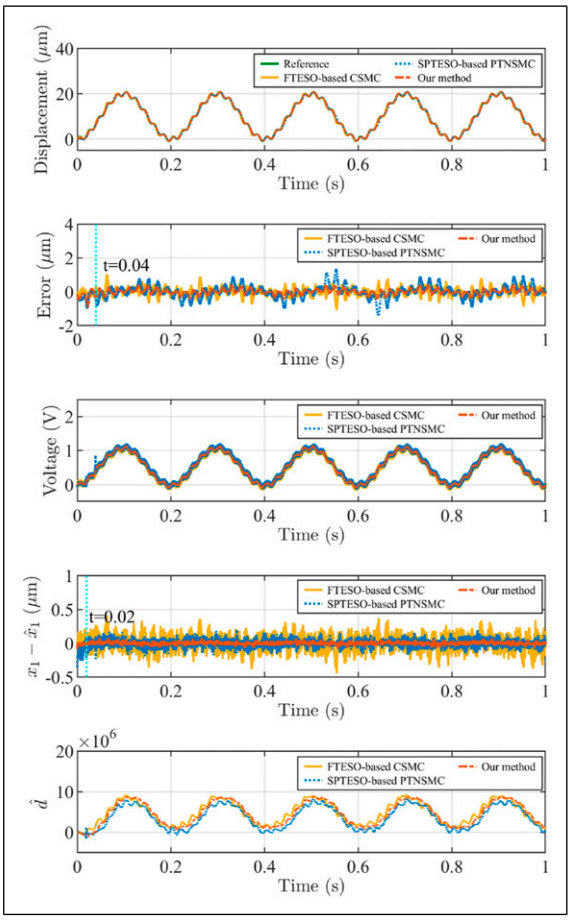

Figure 8. Comparative analysis of experimental results for composite signal trajectory tracking.

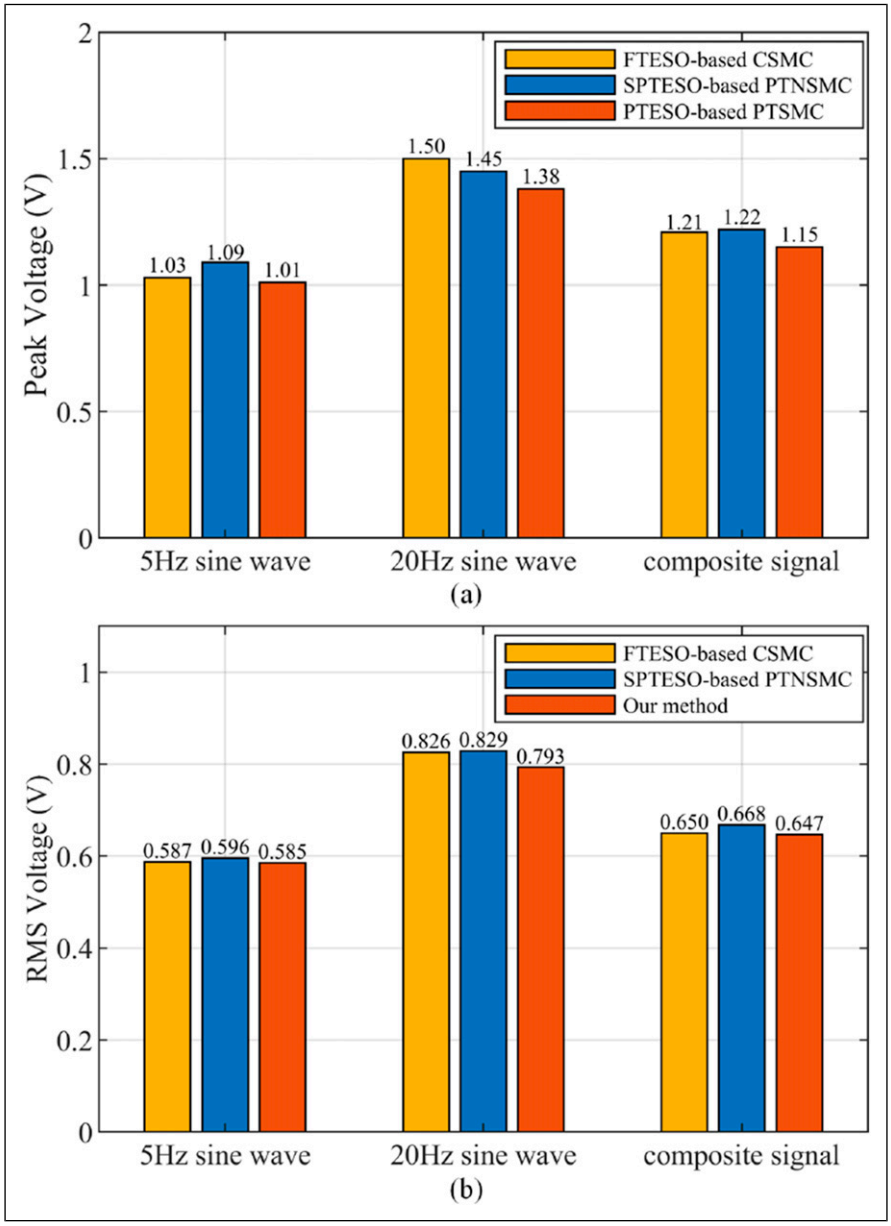

Figure 9. The peak and RMS values of the control input.

Figure 7 further illustrates the experimental results for high-frequency (20 Hz) sine trajectory tracking. A comprehensive analysis of Figure 7 and Table 2 reveals that the maximum tracking errors for the three methods are: 2.547 for FTESO-based CSMC, 3.438 for SPTESO-based PTNSMC, and only 0.694 for the proposed method. This data indicates that even under high-frequency operating conditions, the proposed method maintains the user-defined prescribed-time stability, and its MPTE is reduced by 72.8% and 79.8% compared to the FTESO-based CSMC and SPTESO-based PTNSMC, respectively. Moreover, as observed from the estimation error profiles, the maximum estimation errors of the FTESO and SPTESO reach as high as 0.49 and 0.78, respectively, which are significantly higher than the 0.15 achieved by the proposed PTESO. It can be inferred that the proposed method exhibits optimal tracking robustness and estimation performance across sine reference signals of varying frequencies.

Additionally, to verify the algorithm's capability to handle complex operating conditions, Figure 8 presents a comparison of the tracking performance of the three controllers for a composite signal. According to the statistical data in Figure 8 and Table 2, the maximum tracking errors of the nanopositioning stage under the three control schemes are 0.891 (FTESO-based CSMC), 1.348 (SPTESO-based PTNSMC), and only 0.443 (proposed PTESO-based PTSMC). Meanwhile, Figure 8 shows that the position estimation error achieved by the proposed

observer is as low as 0.083, representing an improvement in observation precision of 79.5% and 59.1% compared to FTESO and SPTESO, respectively. Moreover, the proposed observer is free from the sign function, which eliminates high-frequency switching and results in smoother state estimation. Consequently, it is evident that the proposed control strategy maintains superior dynamic performance even when dealing with complex reference trajectories.

Furthermore, Table 2 also presents the integral absolute error (IAE) and integral time absolute error (ITAE) for the three control methods to evaluate the cumulative tracking performance. It is observed that the proposed control scheme consistently achieves the minimum IAE and ITAE values across all test scenarios. This further corroborates its significant advantages in terms of high precision, minimal error accumulation, and rapid convergence, particularly in the presence of inherent hysteresis nonlinearities and external disturbances.

The control input (Voltage) profiles presented in Figures 6–8 depict the performance of the proposed control scheme. Due to the use of a discontinuous time-varying function in the SPTESO-based PTNSMC method, its control input exhibits pronounced fluctuations at the observer estimation time of 0.02 and the sliding mode stabilization time of 0.04. In contrast, the proposed approach effectively suppresses control input chattering by incorporating a continuous time-varying function and a hyperbolic tangent function, thereby enhancing control smoothness compared to the other two methods. Furthermore, Figure 9 illustrates the peak and root mean square (RMS) values of the control input. It is evident from the figure that our method yields the lowest peak and RMS values. This indicates that the proposed control method significantly reduces control energy consumption and the risk of actuator saturation while achieving superior tracking performance, thereby demonstrating higher engineering practicality.

5. Conclusion

In this paper, we present a prescribed-time sliding mode control (PTSMC) method that integrates a novel prescribed-time extended state observer (PTESO) to solve the high-precision trajectory tracking problem for piezoelectric nanopositioning stages. The PTESO, based on a continuous and bounded time-varying scaling function, is proposed to achieve accurate estimation of the lumped disturbance within a user-defined time to obviate the switching mechanisms that often introduce complexity and instability. Based on robust estimation, we developed a chattering-free PTSMC by replacing the sign function with a hyperbolic tangent function. The resulting integrated controller guarantees system state convergence within a pre-assigned time while maintaining a smooth control signal, which is critical for the longevity and performance of piezoelectric actuators. Comprehensive simulation and experimental results demonstrated that the proposed method outperforms existing finite-time and prescribed-time controllers in both convergence speed and tracking accuracy, while effectively eliminating the control chattering phenomenon. Thus, this work offers a robust and practical solution for high-performance nanopositioning applications. Future work will explore multi-input multi-output nanopositioning systems and investigate adaptive parameter tuning and input saturations.

ORCID iDs

Bo Wang https://orcid.org/0000-0001-6047-1400
Guangwei Wang https://orcid.org/0000-0002-1794-0619

Funding

The authors disclosed receipt of the following financial support for the research, authorship, and/or publication of this article: This research was funded by the National Natural Science Foundation of China under Grant 52265070 and Zhuhai Industry-Academia Cooperation R&D Project under Grant 2320004002732.

Declaration of conflicting interests

The authors declared no potential conflicts of interest with respect to the research, authorship, and/or publication of this article.

Note

1. We use the subscript i to distinguish the functions Γi, each associated with a different convergence time Ti and μi.

References

Chen Z, Ju X, Wang Z, et al. (2022) The prescribed time sliding mode control for attitude tracking of spacecraft. *Asian Journal of Control* 24(4): 1650–1662. https://doi.org/10.1002/asjc.2569

Chen L, Wu Z and Xu Q (2024) Novel adaptive global observer-based sliding mode control of a 2-dof piezoelectric nanopositioning system. *IEEE Transactions on Automation Science and Engineering* 22: 6581–6594. https://doi.org/10.1109/tase.2024.3448249

Clayton GM, Tien S, Leang KK, et al. (2009) A review of feedforward control approaches in nanopositioning for high-speed spm. *Journal of Dynamic Systems, Measurement, and Control* 131(6): 1–19. https://doi.org/10.1115/1.4000158

Cui L and Jin N (2021) Prescribed-time eso-based prescribed-time control and its application to partial igc design. *Nonlinear Dynamics* 106(1): 491–508. https://doi.org/10.1007/s11071-021-06859-5

Guo G, Gao Z and Dong K (2021) Prescribed-time formation control of surface vessels with asymmetric constraints on los range and bearing angles. *Nonlinear Dynamics* 104: 3701–3712. https://doi.org/10.1007/s11071-021-06462-8

Hua C, Ning P and Li K (2022) Adaptive prescribed-time control for a class of uncertain nonlinear systems. *IEEE Transactions on Automatic Control* 67(11): 6159–6166. https://doi.org/10.1109/tac.2021.3130883

Jia C, Liu X, Jia F, et al. (2025) Prescribed-time nonsingular sliding mode control based on neural network for trajectory tracking of nonlinear systems. *Information Sciences* 701: 121850. https://doi.org/10.1016/j.ins.2024.121850

Li J, Liu J, Huangfu S, et al. (2023) Leader-follower formation of light-weight uavs with novel active disturbance rejection control. *Applied Mathematical Modelling* 117: 577–591. https://doi.org/10.1016/j.apm.2022.12.032

Li S, Yang J, Iwasaki M, et al. (2025) Hierarchical disturbance/uncertainty estimation and attenuation for integrated modeling and motion control: overview and perspectives. *IEEE/ASME Transactions on Mechatronics* 30(6): 4435–4449. https://doi.org/10.1109/tmech.2024.3515084

Lv X, Niu Y and Song J (2021) Finite-time boundedness of uncertain hamiltonian systems via sliding mode control approach. *Nonlinear Dynamics* 104(1): 497–507. https://doi.org/10.1007/s11071-021-06292-8

Lyu Z and Xu Q (2022) Design of a new bio-inspired dual-axis compliant micromanipulator with millimeter strokes. *IEEE Transactions on Robotics* 39(1): 470–484. https://doi.org/10.1109/tro.2022.3192778

Pal AK, Kamal S, Nagar SK, et al. (2020) Design of controllers with arbitrary convergence time. *Automatica* 112: 108710. https://doi.org/10.1016/j.automatica.2019.108710

Polyakov A (2012) Nonlinear feedback design for fixed-time stabilization of linear control systems. *IEEE Transactions on Automatic Control* 57(8): 2106–2110. https://doi.org/10.1109/tac.2011.2179869

Shi S, Dai L, Min H, et al. (2024) Non-singular terminal sliding mode controller design for nonlinear systems with prescribed convergence time guarantees. *International Journal of Robust and Nonlinear Control* 34(4): 2597–2613. https://doi.org/10.1002/rnc.7104

Song Z and Sun K (2022) Prescribed performance tracking control for a class of nonlinear system considering input and state constraints. *ISA Transactions* 119: 81–92. https://doi.org/10.1016/j.isatra.2021.02.029

Song Y, Wang Y and Krstic M (2019) Time-varying feedback for stabilization in prescribed finite time. *International Journal of Robust and Nonlinear Control* 29(3): 618–633. https://doi.org/10.1002/rnc.4084

Song Y, Ye H and Lewis FL (2023) Prescribed-time control and its latest developments. *IEEE Transactions on Systems, Man, and Cybernetics: Systems* 53(7): 4102–4116. https://doi.org/10.1109/tsmc.2023.3240751

Song Z, Liu J and Sun K (2025) Performance-guaranteed fault tolerant control for euler–lagrange systems with actuator faults and uncertain disturbance. *Proceedings of the Institution of Mechanical Engineers - Part I: Journal of Systems & Control Engineering* 239(7): 1279–1291. https://doi.org/10.1177/09596518251322239

Sui B, Zhang J and Liu Z (2025) Extended state observer based prescribed-time trajectory tracking control for usv with prescribed performance constraints and input saturation. *Ocean Engineering* 316: 120005. https://doi.org/10.1016/j.oceaneng.2024.120005

Sun G, Ren X, Chen Q, et al. (2015) A modified dynamic surface approach for control of nonlinear systems with unknown input dead zone. *International Journal of Robust and Nonlinear Control* 25(8): 1145–1167. https://doi.org/10.1002/rnc.3127

Tao Y, Li L, Li HX, et al. (2022) High-bandwidth tracking control of piezoactuated nanopositioning stages via active modal control. *IEEE Transactions on Automation Science and Engineering* 19(4): 2998–3006. https://doi.org/10.1109/tase.2021.3104478

Wang G and Xu Q (2017) Design and precision position/force control of a piezo-driven microinjection system. *IEEE/ASME Transactions on Mechatronics* 22(4): 1744–1754. https://doi.org/10.1109/tmech.2017.2698139

Wang B, Wang W, Wang Y, et al. (2017) Dynamical modeling and analysis of viscoelastic properties of single cells. *Micromachines* 8(6): 171. https://doi.org/10.3390/mi8060171

Wang G, Wang B and Zhang C (2021) Fixed-time third-order super-twisting-like sliding mode motion control for piezoelectric nanopositioning stage. *Mathematics* 9(15): 1770. https://doi.org/10.3390/math9151770

Wang G, Wang B, Zhao J, et al. (2023a) Robust tracking for nanopositioning stages using sliding mode control with active disturbance rejection: design and implementation. *Journal of Vibration and Control* 29(15–16): 3809–3822. https://doi.org/10.1177/10775463221106016

Wang G, Zhou Y, Ni L, et al. (2023b) Global fast non-singular terminal sliding-mode control for high-speed nanopositioning. *ISA Transactions* 136: 560–570. https://doi.org/10.1016/j.isatra.2022.10.028

Xu Q (2017) Continuous integral terminal third-order sliding mode motion control for piezoelectric nanopositioning system. *IEEE/ASME Transactions on Mechatronics* 22(4): 1828–1838. https://doi.org/10.1109/tmech.2017.2701417

Yang X, Zhu L, Li S, et al. (2020) Development of a novel pile-up structure based nanopositioning mechanism driven by piezoelectric actuator. *IEEE/ASME Transactions on Mechatronics* 25(2): 502–512. https://doi.org/10.1109/tmech.2020.2972273

Zeng D, Cai C, Liu Y, et al. (2025a) Practical prescribed-time control for underactuated marine surface vessels: theory and experiment. *IEEE Transactions on Automation Science and Engineering* 22: 14074–14083. https://doi.org/10.1109/tase.2025.3557510

Zeng D, Liang Y, Liu Y, et al. (2025b) Adaptive prescribed-time control for marine surface vehicles: a time-varying gain approach. *Journal of Field Robotics* 42(5): 1861–1873. https://doi.org/10.1002/rob.22481

Zhao K, Song Y and Wang Y (2019) Regular error feedback based adaptive practical prescribed time tracking control of normal-form nonaffine systems. *Journal of the Franklin Institute* 356(5): 2759–2779. https://doi.org/10.1016/j.jfranklin.2019.02.015

Zhao Y, Liu Y, Wen G, et al. (2020) Edge-based finite-time protocol analysis with final consensus value and settling time estimations. *IEEE Transactions on Cybernetics* 50(4): 1450–1459. https://doi.org/10.1109/tcyb.2018.2872806